

## Heterogeneous Catalysis

International Edition: DOI: 10.1002/anie.201909551  
German Edition: DOI: 10.1002/ange.201909551

## The Critical Role of Reductive Steps in the Nickel-Catalyzed Hydrogenolysis and Hydrolysis of Aryl Ether C–O Bonds

Meng Wang, Yuntao Zhao, Donghai Mei,\* R. Morris Bullock, Oliver Y. Gutiérrez, Donald M. Camaioni, and Johannes A. Lercher\*

**Abstract:** The hydrogenolysis of the aromatic C–O bond in aryl ethers catalyzed by Ni was studied in decalin and water. Observations of a significant kinetic isotope effect ( $k_H/k_D = 5.7$ ) for the reactions of diphenyl ether under  $H_2$  and  $D_2$  atmosphere and a positive dependence of the rate on  $H_2$  chemical potential in decalin indicate that addition of H to the aromatic ring is involved in the rate-limiting step. All kinetic evidence points to the fact that H addition occurs concerted with C–O bond scission. DFT calculations also suggest a route consistent with these observations involving hydrogen atom addition to the ipso position of the phenyl ring concerted with C–O scission. Hydrogenolysis initiated by H addition in water is more selective (ca. 75%) than reactions in decalin (ca. 30%).

Activation of the aryl C–O bond in aromatic ethers is a necessary step for lignin depolymerization<sup>[1]</sup> and a versatile synthetic strategy for cross-coupling of aryl groups.<sup>[2]</sup> However, the reaction routes, that is, hydrogenolysis and hydrolysis, as well as the competing hydrogenation routes (which saturate the aromatic rings without changing the molecular backbone) are challenging to control.<sup>[3]</sup> Thus, selective aromatic C–O bond cleavage is highly important for remov-

ing an oxygen-based directing group from an aryl ring as well as for the synthesis of fuels and fine chemicals from biomass.<sup>[4]</sup> Transition-metal catalysts, both heterogeneous and homogeneous, have been reported for oxidative and reductive cleavage of C–O bonds.<sup>[2b,5]</sup>

Homogeneous and heterogeneous Ni catalysts selectively catalyze hydrogenolysis of aryl ethers in the liquid phase.<sup>[4f,6]</sup> Some mechanisms have been proposed to be initiated by C–O bond scission followed by H addition to the fragments.<sup>[4b,c,f]</sup> Nevertheless, for heterogeneous catalysts, the high selectivity for hydrogenolysis, and the high reactivity in polar and non-polar phases,<sup>[4d,6b,7]</sup> has not been explained by the accepted mechanisms.

Diphenyl ether has been widely used as model compound for investigating the selective cleavage of aryl ether bonds. Its symmetric structure simplifies product analysis, and the strong bond dissociation energy provides a challenging substrate for catalyst development.<sup>[4d,f-h,8]</sup> The pathways of reductive conversion of diphenyl ether ( $Ph_2O$ ) have been broadly classified into hydrogenolysis, hydrogenation, and reductive hydrolysis.<sup>[4g]</sup> For clarity, we consider hydrogenation to be the sequence of reactions that saturate the aromatic rings (producing cyclohexyl phenyl ether and dicyclohexyl ether), hydrogenolysis to be the reactions that produce  $C_6$  hydrocarbons (e.g., benzene and cyclohexane) and  $C_6$  oxygenates (e.g., phenol, cyclohexanone, and cyclohexanol) in 1:1 ratio, and reductive hydrolysis to be the reactions that produce only  $C_6$  oxygenates.

As the catalytic reductive conversion of  $Ph_2O$  on heterogeneous catalysts always leads to a mixture of products from hydrogenolysis and hydrogenation,<sup>[4a,6b]</sup> the initial rate of H addition to the aromatic ring (upper route in Scheme 1) is comparable to, or even faster than, the C–O bond scission (lower route in Scheme 1). This raises the question of whether the H addition occurs after the C–O bond scission, as reported in homogeneous catalysis.<sup>[4f]</sup> Since we have discovered that the C–O bond in  $Ph_2O$  can be hydrolytically cleaved

[\*] Dr. M. Wang, Dr. R. M. Bullock, Dr. O. Y. Gutiérrez, Dr. D. M. Camaioni, Prof. Dr. J. A. Lercher  
Institute for Integrated Catalysis  
Pacific Northwest National Laboratory  
P.O. Box 999, Richland, WA 99352 (USA)  
E-mail: Johannes.Lercher@ch.tum.de

Y. Zhao

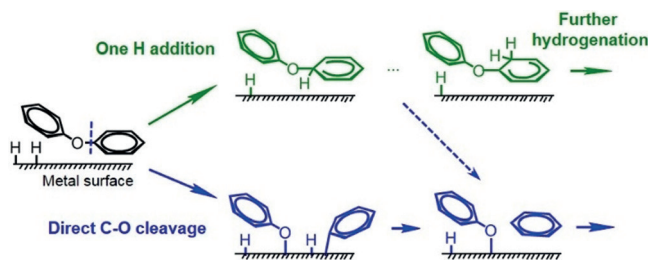
School of Chemical Engineering and Technology  
Tianjin University, Tianjin 300072 (China)

Prof. Dr. D. Mei  
School of Chemistry and Chemical Engineering  
Tianjin Polytechnic University  
Tianjin 300387 (China)  
E-mail: dhmei@tjpu.edu.cn

Prof. Dr. J. A. Lercher  
Department of Chemistry and Catalysis Research Institute  
TU München  
Lichtenbergstrasse 4, 85748 Garching (Germany)

Supporting information and the ORCID identification number(s) for the author(s) of this article can be found under:  
<https://doi.org/10.1002/anie.201909551>.

© 2020 The Authors. Published by Wiley-VCH Verlag GmbH & Co. KGaA. This is an open access article under the terms of the Creative Commons Attribution Non-Commercial NoDerivs License, which permits use and distribution in any medium, provided the original work is properly cited, the use is non-commercial, and no modifications or adaptations are made.



**Scheme 1.** Initial steps proposed for the hydrogenation and hydrogenolysis of diphenyl ether on a metal surface.

after partial hydrogenation of the aromatic ring on Pd,<sup>[4g,h]</sup> an alternative consideration is that hydrogenolysis of the aromatic C–O bond occurs concerted with or following hydrogen addition to the aromatic ring (dashed line in Scheme 1).

Herein, we show the reaction paths on Ni/SiO<sub>2</sub> in polar (water) and non-polar (decalin) solvents in the presence of H<sub>2</sub>, combining kinetic studies (including isotope labeling) with density functional theory (DFT) calculations to derive a detailed molecular account of the reaction steps (Scheme 1). The results indicate that hydrogen addition to the aromatic ring is kinetically relevant to the hydrogenolysis route. The addition of H occurs at higher rates in decalin than in water without changes in the reaction mechanism, although lower apparent activation energies and higher selectivities to hydrogenolysis were observed in the aqueous phase than in decalin. (The reaction conditions are described in the Figure captions and Table footnotes. Details for experimental procedures and DFT calculations are provided in the Supporting Information.)

Powder XRD showed Ni to be present as crystalline metallic particles, and the fractional exposure of metal was 7% by H<sub>2</sub> chemisorption measurements (see the characterization details in the Supporting Information). Ph<sub>2</sub>O was fully converted after 10 h in water (turnover number (TON) = 650) or after 4 h in decalin (TON = 1300), while products from C–O cleavage, that is, C<sub>6</sub> hydrocarbons (benzene and cyclohexane) and C<sub>6</sub> oxygenates (phenol, cyclohexanone, and cyclohexanol), and hydrogenation, that is, cyclohexyl phenyl ether (CyOPh) and dicyclohexyl ether (Cy<sub>2</sub>O), were observed in both solvents (Figure 1). Cyclohexanol was a major constituent of the C<sub>6</sub> oxygenates, and the selectivities to benzene and cyclohexane varied over the course of the reaction (Figures S1 and S2) because of secondary reactions, that is, hydrogenolysis and hydrolysis of CyOPh and hydrogenation of phenol, cyclohexanone, and benzene.

While the same products are produced in either water or decalin, the product distribution is substantially different. In water, C–O cleavage is the dominant reaction, and the selectivity of C<sub>6</sub> oxygenates exceeds the selectivity of C<sub>6</sub> hydrocarbons (Figure 1a). As hydrogenolysis of Ph<sub>2</sub>O generates equal amounts of phenol and benzene, the additional yield of C<sub>6</sub> oxygenates is attributed to hydrolysis of Ph<sub>2</sub>O and CyOPh.<sup>[4e]</sup> The yields of CyOPh, C<sub>6</sub> oxygenates, and C<sub>6</sub> hydrocarbons increased with time up to 90% conversion of Ph<sub>2</sub>O, after which the yield of CyOPh decreased while the yield of C<sub>6</sub> oxygenates increased, and the yield of C<sub>6</sub>

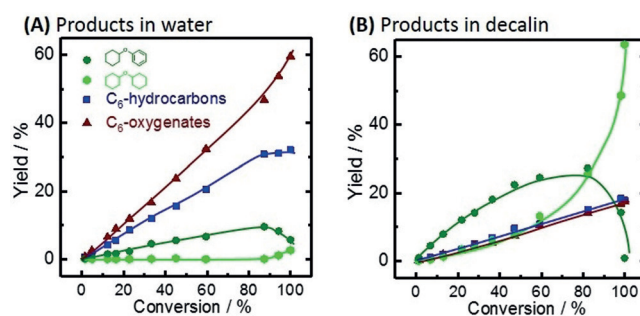


**Figure 1.** Product distributions as a function of conversion of diphenyl ether over Ni/SiO<sub>2</sub> in water (A) and decalin (B) under the same reaction conditions: Diphenyl ether (1.70 g), 64 wt% Ni/SiO<sub>2</sub> catalyst (20 mg in water and 10 mg in decalin), solvent (80 mL water or 40 mL decalin), stirring at 700 rpm, 150°C, H<sub>2</sub> pressure ca. 59 bar. C<sub>6</sub> hydrocarbons represent benzene and cyclohexane; C<sub>6</sub> oxygenates represent phenol, cyclohexanone, and cyclohexanol. The reactions in water and decalin were carried out for 10 and 4 hours, respectively. Detailed time–yield plots and distributions of the reaction pathways are shown in Figures S1 and S2.

hydrocarbons levelled off. This behavior indicates that the selectivity for hydrolysis increased when CyOPh was converted (Figure S1).

Reactions in decalin yielded predominantly hydrogenation products (CyOPh and Cy<sub>2</sub>O). The C<sub>6</sub> oxygenates and C<sub>6</sub> hydrocarbons were produced in approximately equal amounts, reflecting the absence of hydrolysis (Figure 1b). CyOPh was the major product at below 60% conversion. As CyOPh also underwent hydrogenolysis and hydrogenation, the overall selectivity of hydrogenolysis slightly increased from 29% at low conversion to 35% at full conversion (Figure S2).

To focus on the initial reactions of Ph<sub>2</sub>O and minimize secondary reactions, we measured the TOFs of Ph<sub>2</sub>O and the selectivity in water and decalin at conversions less than 20% (Table 1). The selectivities to the three pathways, hydrogenolysis, hydrogenation, and hydrolysis, were calculated from the product distribution. In water, at 150°C and 59 bar H<sub>2</sub> (Table 1, entry 1), the high selectivity to benzene (36%) indicates that hydrogenolysis was the dominant reaction route (72%). The selectivity to phenol (6%) is lower than that to benzene because phenol was hydrogenated faster than benzene.<sup>[6b]</sup> The overall higher selectivity (53%) to C<sub>6</sub> oxygenates (6% phenol, 4% cyclohexanone, and 43% cyclohexanol) than to C<sub>6</sub> hydrocarbons (mainly benzene) showed

**Table 1:** Reactions of diphenyl ether on Ni/SiO<sub>2</sub> in water and decalin solvents under hydrogen gas.<sup>[a]</sup>

Entry	Solvent	H <sub>2</sub> [bar]	TOF <sup>[b]</sup> [h <sup>-1</sup> ]	Product carbon selectivity [%]						Reaction route selectivity <sup>[c]</sup> [%]			
											Hydrogenolysis	Hydrogenation	Hydrolysis
1	water	58.6	140	36	–	6	4	43	11	–	72	11	17
2	decalin	59.5	830	5	10	1	–	13	61	10	29	71	–
3	decalin	17.3	290	16	2	1	–	16	57	8	35	65	–
4	decalin	6.2	160	15	6	1	–	20	56	2	42	58	–

[a] Reaction conditions: Reactant (1.70 g), 64 wt% Ni/SiO<sub>2</sub> catalyst (10 mg), solvent (80 mL water or 40 mL decalin), 150°C, stirring at 700 rpm. Hydrogen pressure was corrected to 150°C (see details in the Supporting Information). [b] Calculated at <20% conversion. [c] Hydrogenolysis = 2 × (cyclohexane + benzene); hydrolysis = (phenol + cyclohexanone + cyclohexanol) – hydrogenolysis; hydrogenation = (phenyl cyclohexyl ether + dicyclohexyl ether).

that hydrolysis also occurred to an extent of approximately 17%.

Ph<sub>2</sub>O reacted six times faster in decalin (Table 1, entry 2; TOF = 830 h<sup>-1</sup>) than in water (Table 1, entry 1; TOF = 140 h<sup>-1</sup>) under the same conditions. Hydrogenation was the dominant reaction route (71%) and only hydrogenolysis contributed to the minor products (29%) as hydrolysis does not occur in the absence of water (equal amounts of C<sub>6</sub> oxygenates and C<sub>6</sub> hydrocarbons were produced). To study the effect of H<sub>2</sub> pressure on rate and selectivity, we also performed reactions at 17.3 bar and 6.2 bar H<sub>2</sub> (Table 1, entries 3 and 4). The four major products, namely benzene (5–16%), cyclohexanol (13–20%), CyOPh (56–61%), and Cy<sub>2</sub>O (2–10%), were all obtained at all H<sub>2</sub> pressures (6–60 bar). Hydrogenation (58–71%) remained the dominant route even at the lowest H<sub>2</sub> pressure.

Control experiments were performed with the initial products, benzene, phenol, and CyOPh, from Ph<sub>2</sub>O to investigate the secondary reactions (Table S1). Compared to the TOF observed from Ph<sub>2</sub>O (290 h<sup>-1</sup>) at 150 °C and 17.3 bar of H<sub>2</sub> in decalin, the TOFs using phenol as a substrate were one order of magnitude higher in the presence (1700 h<sup>-1</sup>) or absence (2100 h<sup>-1</sup>) of Ph<sub>2</sub>O; the TOFs of other initial products, CyOPh (110 h<sup>-1</sup>) and benzene (120 h<sup>-1</sup>), were comparable to that of Ph<sub>2</sub>O. The fast hydrogenation of phenol explains its low yield in reactions of Ph<sub>2</sub>O and CyOPh even though phenol is an initial product from hydrogenolysis of Ph<sub>2</sub>O. In water, the rate of phenol conversion was also higher (660 h<sup>-1</sup>) than that of Ph<sub>2</sub>O (140 h<sup>-1</sup>), whereas the rates of conversion of other small compounds were lower than that of Ph<sub>2</sub>O.

In summary, the same products were formed in water and in decalin, though with different distributions. Hydrogenation and hydrogenolysis are significant routes in both solvents, while selectivity for hydrogenation is greater in decalin, in part because hydrolysis cannot occur. In what follows, we elucidate details of the reaction mechanism for hydrogenolysis.

Hydrogenolysis is favored by lower pressures of H<sub>2</sub> in decalin (Figure 2a). Commensurately, the reaction orders in H<sub>2</sub> for Ph<sub>2</sub>O hydrogenolysis and hydrogenation were 0.4 and 0.8, respectively, in the pressure range 3.3–90 bar H<sub>2</sub> (Figure 2a). The constant and positive reaction order over a 27-fold variation in H<sub>2</sub> pressure indicates that the H surface

coverage was relatively low under these conditions. The observation that hydrogenolysis was approximately half order in H<sub>2</sub>, while hydrogenation was first order in H<sub>2</sub>, suggests a mechanism in which one H atom is added before or during the rate-determining step of the hydrogenolysis pathway.<sup>[9]</sup> We rule out that H addition following C–O bond scission is rate-determining because hydrogen addition to the adsorbed fragments, that is, phenyl or phenoxy, is rapid,<sup>[10]</sup> and thus is not expected to limit the rate of hydrogenolysis.

To test the hypothesis that H addition is rate-limiting for hydrogenolysis, deuterium kinetic isotope effect and tracer studies were performed in decalin where only hydrogenation and hydrogenolysis pathways occur and H/D exchange with D<sub>2</sub> is negligible. The reaction in water is not reported because of the rapid exchange between D<sub>2</sub> and H<sub>2</sub>O, D<sub>2</sub>O with Ph<sub>2</sub>O, and D<sub>2</sub>O with reaction products. Consistent with the H<sub>2</sub> kinetic orders observed above, we measured significant kinetic isotope effects of 5.7 and 4.8 (Table 2) for hydrogenolysis and hydrogenation, respectively. This is perfectly reflected by our DFT-calculated *k*<sub>H</sub>/*k*<sub>D</sub> value of 5.7 for the Ni–H bond cleavage (see details in the Supporting Information). Thus, we conclude that hydrogen is involved in the rate-determining step of the C–O bond scission.

To support the assignment of these effects to H addition steps, we first note that H/D exchange between H<sub>2</sub> and D<sub>2</sub> equilibrated in the time interval required to reach reaction temperature (Figure S3). Thus, diffusion and activation of H<sub>2</sub>/D<sub>2</sub> on the metal surface are concluded not to be rate-limiting steps. Second, even though H/D exchange occurred between D<sub>2</sub> and reactants/products, the abundance of D in D<sub>2</sub>, HD, and H<sub>2</sub> (gas phase) never fell below 82% (Figure S4). Conversions of the reactant in H/D exchange and reductive consumption were below 5% (Figure S4). Lastly, the product distribution and selectivity were very similar for H<sub>2</sub> and D<sub>2</sub> (Figures S5 and S6). Therefore, the initial rates of the hydrogenolysis and hydrogenation of Ph<sub>2</sub>O are reliable measures of the isotope effects. We attribute the primary isotope effects to the cleavage of Ni–H versus Ni–D bonds in the transition states of rate-limiting steps for hydrogenolysis and hydrogenation.

For evidence that the kinetic isotope effect involves H addition to Ph<sub>2</sub>O, we traced the positions into which D was incorporated in benzene, phenol, and unreacted Ph<sub>2</sub>O. One D was found in benzene (C<sub>6</sub>H<sub>5</sub>D > 90%) and no D was found in the aromatic ring of phenol C<sub>6</sub>H<sub>5</sub>OD (> 90%; see Figure S7). Hence, the products from hydrogenolysis in D<sub>2</sub> were con-

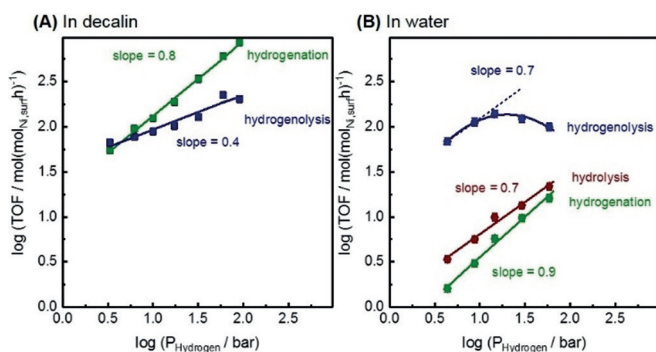


**Figure 2.** Hydrogen dependencies for the reactions of diphenyl ether over Ni/SiO<sub>2</sub> in decalin (A) and water (B). The H<sub>2</sub> pressure varied from 3.3 to 90 bar in decalin and from 4.4 to 59 bar in water.

**Table 2:** Reaction rates and the corresponding isotope effects observed for the conversion of diphenyl ether with H<sub>2</sub> or D<sub>2</sub>.<sup>[a]</sup>

	Gas	Hydrogenolysis	Hydrogenation	Deuteration <sup>[b]</sup>
TOF [h <sup>-1</sup> ]	H <sub>2</sub>	68 ± 5	95 ± 5	
TOF [h <sup>-1</sup> ]	D <sub>2</sub>	12 ± 3	20 ± 4	35 ± 5
KIE <sub>H/D</sub>		5.7	4.8	

[a] Reaction conditions: Diphenyl ether (1.70 g), 64 wt% Ni/SiO<sub>2</sub> catalyst (10 mg), 40 mL decalin, 150 °C, gas pressure 6.2 bar at 150 °C, stirring at 700 rpm. TOFs were calculated at < 20% conversion. [b] Rate of the deuteration of diphenyl ether from the H/D exchange between diphenyl ether and D<sub>2</sub> (Figure S4). Deuteration at the *o*-, *m*-, and *p*-positions was quantified by <sup>2</sup>H NMR analysis (Figure S8); the *o*/*m*/*p* distribution is 1:2:1.

cluded to be  $C_6H_5D$  and  $C_6H_5OD$  (Figure S7). This indicates that only one H atom is added to the phenyl ring before or concerted with C–O bond scission.

The H/D exchange between  $Ph_2O$  and  $D_2$  shows that H addition to the aromatic ring is reversible. The rates of H/D exchange (deuteration) are competitive with the rates of formation of the products (Table 2 and Figure S4). The distribution of D in the recovered  $Ph_2O$  is non-statistical, that is, the proportion of D at the *ortho*, *meta*, and *para* positions is approximately 1:2:1 (Figure S8). This low level of D incorporation at the *ortho* position could indicate that the *o*-D adduct is less favorably formed, or that the *o*-D adduct is converted into products more rapidly than the *m*- and *p*-D adducts. In support of the latter, density functional theory calculations (Table S2) find that the *o*- and *m*-H adducts are energetically favored over the *p*-H adduct by 17–18  $\text{kJ mol}^{-1}$ , while the barriers to forming the *o*- and *p*-H adducts are lower than the barrier to form the *m*-H adduct by 13–14  $\text{kJ mol}^{-1}$ . Addition of H to the carbon bonded to the OPh group (*ipso* position) did not produce a stable surface-adsorbed H adduct.

An energy diagram calculated by DFT is shown in Figure 3 for the hydrogenolysis and hydrogenation pathways (the corresponding structures are provided in Table S3). For hydrogenation, the stepwise addition of three hydrogen atoms via the initially formed *o*-H adduct is shown. For hydrogenolysis, two routes are considered, namely 1) C–O bond breaking concerted with phenyl–H bond formation (H-assisted) and 2) stepwise “hydrogen addition first (at the *ortho* position)” followed by C–O bond cleavage. The concerted C–O bond cleavage mechanism (orange line) has a higher activation barrier of 200  $\text{kJ mol}^{-1}$ . Stepwise hydrogen addition followed by C–O bond cleavage via the *o*-H adduct has an overall barrier of 189  $\text{kJ mol}^{-1}$  (black line) comprising the energy of formation (52  $\text{kJ mol}^{-1}$ ) of the *o*-H adduct and the barrier (137  $\text{kJ mol}^{-1}$ ) for subsequent C–O bond scission. The concerted pathway initiated by *ipso* attack of a surface H atom is consistent with experimental observations of approximately half-order rate dependence on  $H_2$  and a sig-

nificant  $H_2/D_2$  KIE. The stepwise route would be consistent, too, provided the back-reaction of the H adduct to  $Ph_2O$  (H elimination) is competitive with C–O scission, which could be the case if the frequency factor for C–O scission is sufficiently greater than the frequency factor for H elimination. Thus, we do not exclude this route.

After the first hydrogen addition, the second H addition (103–133  $\text{kJ mol}^{-1}$ ) is, however, kinetically easier than the C–O bond scission (137  $\text{kJ mol}^{-1}$ ). Also, the third consecutive H addition step, with a low barrier of 69  $\text{kJ mol}^{-1}$ , is feasible. This is consistent with the experimental observation of a first-order reaction in  $H_2$  for hydrogenation and the relatively high selectivity to hydrogenation products in decalin. The apparent activation energies for hydrogenolysis and hydrogenation in decalin were 101 and 77  $\text{kJ mol}^{-1}$ , respectively (Figure S9). The higher activation enthalpy for hydrogenolysis compared to hydrogenation agrees well with the DFT calculations.

In water, a different hydrogen dependence was observed for hydrogenolysis. Although the relations between the logarithmic rates of hydrogenation and hydrolysis and the logarithm of  $H_2$  pressure were linear with slopes of 0.9 and 0.7, respectively, over the  $H_2$  pressure range of 4.4–59 bar (Figure 2b), the dependence of the logarithm of the hydrogenolysis rate on the logarithm of  $H_2$  pressure was not. The  $H_2$  dependence for hydrolysis, near first order, is similar to that observed on Pd catalysts.<sup>[46]</sup> Thus, we hypothesize that hydrolysis is initiated by partial hydrogenation of  $Ph_2O$  to the enol ether, cyclohex-1-enyl phenyl ether, which is converted into phenol and cyclohexanone. For hydrogenolysis over the range of 4.4–15 bar  $H_2$ , the TOF increased, and then decreased above 29 bar. Initially, the reaction order in  $H_2$  is like that for hydrolysis, indicating that hydrogen is transferred to  $Ph_2O$  before or concerted with the C–O bond cleavage.

The reasons for the reaction order in  $H_2$  to turn negative above 15 bar are unclear at present. Hydrogen addition to carbon–carbon double bonds on Ni is usually structure-insensitive,<sup>[11]</sup> while hydrogenolysis of C–C bonds in hydrocarbons is structure-sensitive.<sup>[12]</sup> Thus, we hypothesize that

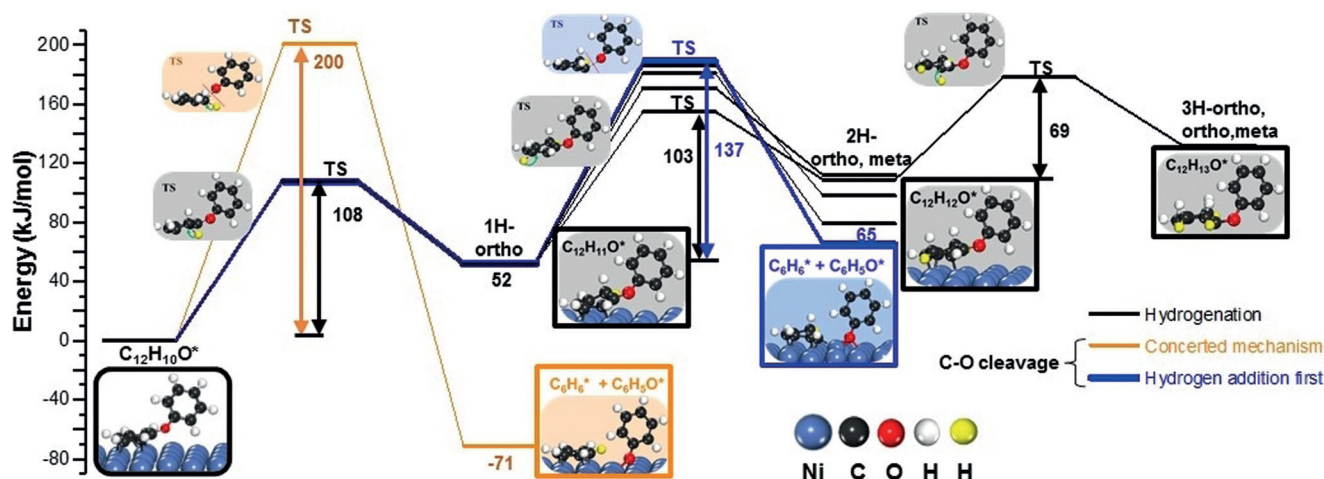


**Figure 3.** Potential energy profiles for the hydrogenolysis and hydrogenation of diphenyl ether over the Ni catalyst. A\* represents the adsorption state of A on the surface. “Concerted mechanism” refers to C–O bond cleavage while a H atom is added to the phenyl ring and “hydrogen addition first” means one hydrogen is added first, which is followed by C–O bond cleavage. Zero-point energy corrections have been applied to initial, transition, and final states. White and yellow spheres are for H originally in diphenyl ether and H from metal surface.

C–O bond cleavage of the H adduct of Ph<sub>2</sub>O, which requires an adjacent vacant site, is also structure-sensitive. We suggest that water may block this vacant site by competitive adsorption, while other sites are more readily saturated by H. Under the high pressures of H<sub>2</sub>, the reaction rate of hydrogenolysis decreases because of a decreasing concentration of H adduct/vacant site pairs, while hydrogenation and hydrolysis, which do not require an adjacent vacant site, still increase in rate with increasing H coverage (Figure S10).

Thus, hydrogenolysis follows the same mechanism in water and in decalin. Hydrogenolysis is initiated by H addition to the aromatic ring, which weakens the aromatic C–O bond. When the reactivities in decalin and water are compared under low H<sub>2</sub> pressures (3.3–15 bar), the hydrogenation rates are much lower in water, while the hydrogenolysis rates are comparable. This is attributed to a lower surface coverage of H in water than in decalin. In contrast, the dissociation of the polar ether C–O bond on Ni in water is more favorable because of stabilization of the transition state. Both compensating effects are, therefore, hypothesized to cause the high selectivity of hydrogenolysis in water.

In conclusion, the high primary kinetic isotope effect ( $KIE_{H/D} > 5$ ), the H<sub>2</sub> pressure dependence for Ni/SiO<sub>2</sub>-catalyzed hydrogenolysis of diphenyl ether, and the DFT-modeled routes corroborate the hypothesis that the hydrogenolytic C–O bond cleavage of an aromatic ether bond on the surface of a Ni particle is initiated by hydrogen addition to the aromatic ring. This mechanism is in stark contrast to reaction routes that are catalyzed by molecular catalysts, where hydrogenolysis is initiated by a rate-determining oxidative addition of aryl ethers to neutral Ni<sup>0</sup>.<sup>[4f]</sup> The first step of hydrogen addition is followed by the ether C–O bond cleavage, which leads to benzene and phenoxyl groups on the metal surface. The present results also indicate that the partial hydrogenation of aromatic rings may be a more general reaction principle for cleaving C–O bonds in alcohols and ethers. This insight, in turn, opens new synthesis pathways that enable selective manipulation of C–O bonds.

## Acknowledgements

This work was supported by the U.S. Department of Energy (DOE), Office of Science, Office of Basic Energy Sciences (BES), Division of Chemical Sciences, Geosciences and Biosciences (Transdisciplinary Approaches to Realize Novel Catalytic Pathways to Energy Carriers, FWP 47319). Portions of the work were performed at the William R. Wiley Environmental Molecular Sciences Laboratory, a national scientific user facility sponsored by the DOE's Office of Biological and Environmental Research located at Pacific Northwest National Laboratory, a multiprogram national laboratory operated for DOE by Battelle Memorial Institute.

## Conflict of interest

The authors declare no conflict of interest.

**Keywords:** catalysis · C–O bond cleavage · hydrogenolysis · nickel · reaction mechanisms

**How to cite:** *Angew. Chem. Int. Ed.* **2020**, *59*, 1445–1449  
*Angew. Chem.* **2020**, *132*, 1461–1465

- [1] a) J. Zakzeski, P. C. A. Bruijninx, A. L. Jongerius, B. M. Weckhuysen, *Chem. Rev.* **2010**, *110*, 3552–3599; b) D. M. Alonso, S. G. Wettstein, J. A. Dumesic, *Chem. Soc. Rev.* **2012**, *41*, 8075–8098.
- [2] a) B. M. Rosen, K. W. Quasdorf, D. A. Wilson, N. Zhang, A.-M. Resmerita, N. K. Garg, V. Percec, *Chem. Rev.* **2011**, *111*, 1346–1416; b) J. Cornella, C. Zarate, R. Martin, *Chem. Soc. Rev.* **2014**, *43*, 8081–8097.
- [3] a) X. Wang, R. Rinaldi, *ChemSusChem* **2012**, *5*, 1455–1466; b) E. M. van Duzee, H. Adkins, *J. Am. Chem. Soc.* **1935**, *57*, 147–151.
- [4] a) A. G. Sergeev, J. F. Hartwig, *Science* **2011**, *332*, 439–443; b) P. Kelley, S. Lin, G. Edouard, M. W. Day, T. Agapie, *J. Am. Chem. Soc.* **2012**, *134*, 5480–5483; c) J. Cornella, E. Gómez-Bengoia, R. Martin, *J. Am. Chem. Soc.* **2013**, *135*, 1997–2009; d) F. Gao, J. D. Webb, J. F. Hartwig, *Angew. Chem. Int. Ed.* **2016**, *55*, 1474–1478; *Angew. Chem.* **2016**, *128*, 1496–1500; e) Q. Meng, M. Hou, H. Liu, J. Song, B. Han, *Nat. Commun.* **2017**, *8*, 14190; f) N. I. Saper, J. F. Hartwig, *J. Am. Chem. Soc.* **2017**, *139*, 17667–17676; g) M. Wang, H. Shi, D. M. Camaioni, J. A. Lercher, *Angew. Chem. Int. Ed.* **2017**, *56*, 2110–2114; *Angew. Chem.* **2017**, *129*, 2142–2146; h) M. Wang, O. Y. Gutiérrez, D. M. Camaioni, J. A. Lercher, *Angew. Chem. Int. Ed.* **2018**, *57*, 3747–3751; *Angew. Chem.* **2018**, *130*, 3809–3813.
- [5] A. Rahimi, A. Ulbrich, J. J. Coon, S. S. Stahl, *Nature* **2014**, *515*, 249.
- [6] a) P. Álvarez-Bercedo, R. Martin, *J. Am. Chem. Soc.* **2010**, *132*, 17352–17353; b) J. He, C. Zhao, J. A. Lercher, *J. Am. Chem. Soc.* **2012**, *134*, 20768–20775; c) M. Zaheer, R. Kempe, *ACS Catal.* **2015**, *5*, 1675–1684; d) V. Molinari, G. Clavel, M. Graglia, M. Antonietti, D. Esposito, *ACS Catal.* **2016**, *6*, 1663–1670; e) J. Zhang, M. Ibrahim, V. Collière, H. Asakura, T. Tanaka, K. Teramura, K. Philippot, N. Yan, *J. Mol. Catal. A* **2016**, *422*, 188–197; f) S. Van den Bosch, T. Renders, S. Kennis, S. F. Koelewijn, G. Van den Bossche, T. Vangeel, A. Deneyer, D. Depuydt, C. M. Courtin, J. M. Thevelein, W. Schutyser, B. F. Sels, *Green Chem.* **2017**, *19*, 3313–3326; g) S. Bulut, S. Siankevich, A. P. van Muyden, D. T. L. Alexander, G. Savoglidis, J. Zhang, V. Hatzimaniakatis, N. Yan, P. J. Dyson, *Chem. Sci.* **2018**, *9*, 5530–5535; h) Z. Sun, B. Fridrich, A. de Santi, S. Elangovan, K. Barta, *Chem. Rev.* **2018**, *118*, 614–678; i) X. Chen, W. Guan, C.-W. Tsang, H. Hu, C. Liang, *Catalysts* **2019**, *9*, 488.
- [7] A. G. Sergeev, J. D. Webb, J. F. Hartwig, *J. Am. Chem. Soc.* **2012**, *134*, 20226–20229.
- [8] H. Zeng, D. Cao, Z. Qiu, C. J. Li, *Angew. Chem. Int. Ed.* **2018**, *57*, 3752–3757; *Angew. Chem.* **2018**, *130*, 3814–3819.
- [9] a) M. L. Toebes, T. Alexander Nijhuis, J. Hájek, J. H. Bitter, A. Jos van Dillen, D. Y. Murzin, K. P. de Jong, *Chem. Eng. Sci.* **2005**, *60*, 5682–5695; b) Z. Zhao, R. Bababrik, W. Xue, Y. Li, N. M. Briggs, D.-T. Nguyen, U. Nguyen, S. P. Crossley, S. Wang, B. Wang, D. E. Resasco, *Nat. Catal.* **2019**, *2*, 431–436.
- [10] J. He, L. Lu, C. Zhao, D. Mei, J. A. Lercher, *J. Catal.* **2014**, *311*, 41–51.
- [11] M. Boudart, W. C. Cheng, *J. Catal.* **1987**, *106*, 134–143.
- [12] A. Sárkány, P. Tétényi, *React. Kinet. Catal. Lett.* **1979**, *12*, 297–301.

Manuscript received: July 29, 2019

Revised manuscript received: September 3, 2019

Accepted manuscript online: September 11, 2019

Version of record online: December 12, 2019